LRP 688/00 December 2000

Steady-state fully non-inductive operation with electron cyclotron current drive and current profile control in the tokamak à configuration variable TCV

O. Sauter and the TCV Team in collaboration with
KFKI, Budapest, HU, TRINITI, Troisk, RUS, Istituto di
Fisica del Plasma "P. Caldirola", Milano, I,
CEA, Cadarache, F, IPP, Prague, CZ

Invited Paper at the 42nd Annual Meeting of
the APS Division of Plasma Physics
combined with the 10th International
Congress on Plasma Physics

Québec City, Canada, October 2000

Submitted for publication to
Physics of Plasmas

ISSN 0458-5895

Steady-state fully non-inductive operation with electron cyclotron current drive and current profile control in the Tokamak à Configuration Variable TCV

O. Sauter, C. Angioni, S. Coda, P. Gomez, T.P., Goodman, M.A. Henderson, F. Hofmann, J.-P. Hogge, J.-M. Moret, P. Nikkola, Z.A. Pietrzyk, H. Weisen, S. Alberti, K. Appert, J. Bakos[1], R. Behn, P. Blanchard, P. Bosshard, R. Chavan, I. Condrea, A. Degeling, B.P. Duval, D. Fasel, J.-Y. Favez, A. Favre, I. Furno, R.R. Kayruthdinov[2], P. Lavanchy, J.B. Lister, X. Llobet, V.E. Lukash[3], P. Gorgerat, P.-F. Isoz, B. Joye, J.-C. Magnin, A. Manini, B. Marlétaz, P. Marmillod, Y. R. Martin, An. Martynov, J.-M. Mayor, E. Minardi[4], J. Mlynar, P.J. Paris, A. Perez, Y. Peysson[5], V. Piffl[6], R.A. Pitts, A. Pochelon, H. Reimerdes, J.H. Rommers, E. Scavino, A. Sushkov[2], G. Tonetti, M.Q. Tran, A. Zabolotsky

Centre de Recherches en Physique des Plasmas
Association Euratom – Confédération Suisse
Ecole Polytechnique Fédérale de Lausanne
CH-1015 Lausanne – Switzerland

[1]KFKI, Budapest, HU; [2]RCC, Moscow, RUS; [3]TRINITI, Troisk, RUS; [4]Istituto di Fisica del Plasma "P. Caldirola", Milano, I; [5]CEA Cadarache, F; [6]IPP, Prague, CZ

Abstract:

Fully non-inductive, steady-state electron cyclotron current drive (ECCD) has been demonstrated for the first time in experiments carried out in the Tokamak à Configuration Variable TCV [O. Sauter *et al.*, Phys. Rev. Lett. **84**, 3322 (2000)]. By appropriately distributing six 0.45MW ECCD sources over the discharge cross section, fully non- inductive, stable and stationary plasmas with I_p up to 210kA were obtained for the full discharge duration of 1.9s, corresponding to more than 900 energy confinement times and more than 10 current redistribution times at an average current drive efficiency $\eta_{20CD}=0.01$ $[10^{20}AW^{-1}m^{-2}]$. These experiments have also demonstrated for the first time the steady recharging of the Ohmic transformer using ECCD only. The effect of localized off-axis electron cyclotron heating (ECH) and EC current drive (ECCD) (co- and counter-) is investigated showing that locally driven currents amounting to only 1% of I_p significantly alter sawtooth periods and crash amplitudes. An improved

quasi- stationary core confinement regime, with little or no sawtooth activity, has been obtained by a combination of off-axis ECH and on-axis CNTR-ECCD.

I. Introduction

Tokamak research has made considerable progress both on the experimental front, in particular in the areas of confinement improvement and long pulse scenarios, and in the theoretical understanding and numerical simulation of tokamak discharges. Both are required for achieving the goals of any next large experimental reactor. Moreover, both have reached such a level of complexity and performance that any future progress is bound to be achieved by combining the two approaches. It is in this perspective that a small to medium size tokamak, such as the Tokamak à Configuration Variable (TCV), can contribute significantly to worldwide fusion research. It is also clear that to obtain the performances necessary for a relevant experimental reactor, both profile control and long pulse operation are very important. In order to address these issues, the TCV tokamak has been designed with very flexible plasma shape control (see Fig. 1) and electron cyclotron (EC) systems, equipped with six 0.45MW gyrotrons at second harmonic, 82.7 GHz, steerable in both the poloidal and toroidal directions (see Fig. 2) [1]. EC heating (ECH) and current drive (ECCD) allows for both global and local profile control. Global profile control was demonstrated with a fully non-inductive discharge of 123kA, $n_{el} \approx 1.10^{19} m^{-3}$, first presented in Ref. 2. Recent developments in these fully non-inductive scenarios and the recharging of the transformer will be presented in Section 2. This is the first instance of global current profile sustainment, with ECCD only, in a reactor relevant regime [3] and is the culmination of results obtained in many different institutions. It is worth citing the sustainment of 3kA with $n_{el} \approx 2 \cdot 10^{18} m^{-3}$ in WT-2 [4], later improved in WT-3 to 70kA, albeit in a low single-pass low confinement scenario [5]. Efficient ECCD at the first harmonic has been first obtained in T-10, with finite $E_{\|}$, with a current-drive efficiency $\eta_{20cD} \approx 0.03$ and an efficiency $\eta_{20cD} \approx 0.01$ in X2-mode in a high performance discharge ($n_{el} \geq 10^{19} m^{-3}$, $T_e \geq 5keV$ at $I_{CD} \approx 110kA$, P=2.5MW) [6]. Further references can be found in the recent review by B. Lloyd *et al.* [7].

Local current or pressure profile tailoring has naturally been the first application of ECH/ECCD, owing in part to the limited power available but also to its large local absorption coefficient and therefore narrow deposition profile. Two examples are the stabilisation of 2/1 tearing modes in T-10 [8] and of the neoclassical tearing mode in ASDEX-U [9]. In TCV, we have studied the effects of local power deposition and current drive on the sawtooth activity and sawtooth period. These results will be presented in Section 3.

Finally we shall present in Section 4 the effect of global pressure and current profile control with ECH/ECCD in order to obtain scenarios with improved electron confinement. As expected, localised deposition in a good confinement region, in the center, improves the confinement even further or, more precisely, drastically reduces the power degradation of the global confinement time. This is encouraging in the perspective of a reactor where the main heating source will be central. In addition, we have found a quasi-stationary improved central electron confinement regime (ICEC) using a combination of off-axis ECH and on-axis counter-current drive (CNTR-CD) [10]. Very good electron transport barriers have already been reported, in particular the results obtained on RTP [11], however these could not be sustained. Other important results of the recent experimental campaign on TCV can be found in Refs [12,13].

II. Fully non-inductive scenario

The ultimate demonstration of an efficient and robust current drive system in a tokamak is its ability to recharge the transformer, that is to be comparable to the main current source. The reversal of the primary transformer current is shown in Fig. 3. Note the steady recharging rate indicating stationary conditions. The toroidal launch angle, φ, can easily be changed on TCV. In most of the discharges presented here, $\varphi \approx 35°$, a value that was shown to be close to optimum while still preserving a weak dependence of the ray trajectories on density [14]. Similarly, the polarization can be modified, however in the results presented here only extraordinary waves launched at second harmonic have been used (X-2 mode). Following the first results presented in Refs. [2] and [3], we have developed steady-state fully non-inductive discharges, in which the inductive component is suppressed by modifying the feedback control such as to keep the

transformer current I_{OT} constant (Fig. 4) [12]. Using this method, up to 210kA have been sustained with six gyrotrons, 2.7MW, $n_{el} \approx 1.3 \cdot 10^{19} m^{-3}$ for a 2s duration limited only by the gyrotron pulse length. This duration is equivalent to over 900 confinement times and 10 current redistribution times, the latter being inferred from the time evolution of the internal inductance l_i and elongation κ [3, 12]. In steady-state, the different contributions to the total plasma current are much easier to determine, using Faraday's law [15]:

$$\frac{\partial B_{pol}}{\partial t} = 0 = \frac{\partial}{\partial \rho} E_0 = \frac{\partial}{\partial \rho} \frac{\langle E_{//} B \rangle}{R_0 \langle \underline{B} \cdot \underline{\nabla} \varphi \rangle}, \tag{1}$$

where ρ is a flux surface radial coordinate. Therefore E_0 is constant over the minor radius. From Ohm's law we have $\langle \mathbf{E}_{//} \cdot \mathbf{B} \rangle = \eta_{neo} (\langle \mathbf{j_{tot}} \cdot \mathbf{B} \rangle - \langle \mathbf{j_{BS}} \cdot \mathbf{B} \rangle - \langle \mathbf{j_{CD}} \cdot \mathbf{B} \rangle)$, where j_{BS} is the bootstrap current and $E_0 = V_{loop} / 2\pi R_0$. On the basis of Eq. (1), we can introduce the natural normalisation for the parallel current:

$$\tilde{j}_A = \frac{\langle \underline{j}_A \cdot \underline{B} \rangle}{R_0 \langle \underline{B} \cdot \underline{\nabla} \varphi \rangle} = \frac{\langle \underline{j}_A \cdot \underline{B} \rangle}{R_0 F \langle 1/R^2 \rangle} \tag{2}$$

$$j_{ohm//} = \sigma_{neo} E_0 = \sigma_{neo} V_{loop} / 2\pi R_0 \tag{3}$$

where $F(\psi) = R B_\varphi$ and A stands for total, BS or CD. From Ampere's law we have:

$$I_A(\psi) = \frac{R_0}{2\pi} F(\psi) \int_0^{\psi} \frac{\langle 1/R^2 \rangle}{F} \tilde{j}_A \, dV \tag{4}$$

$$I_{ohm}^{(\psi)} = \frac{V_{loop}}{4\pi^2} F(\psi) \int_0^{\psi} \frac{\langle 1/R^2 \rangle}{F} \sigma_{neo} \, dV \tag{5}$$

Hence we see that the total plasma conductance $\bar{\sigma} = I_{ohm} / V_{loop}$ is given by:

$$\bar{\sigma} = \frac{F(\psi)}{4\pi^2} \int_0^{\psi_{edge}} \frac{\langle 1/R^2 \rangle}{F} \sigma_{neo} \, dV \tag{6}$$

Using the formula given in Ref. [16] for σ_{neo} and the experimental density and temperature profiles, we find $\bar{\sigma} \approx 3-6\cdot10^5 A/V$ for discharges similar to the ones in Ref. [3], while the value determined experimentally, from direct current and voltage measurements in cases with small but finite $E_{//}$, is around $6\cdot10^5$A/V [3b, 17]. These numbers agree within the error bars, in particular due to the uncertainty on Z_{eff}, however the values calculated from Eq. (6) are systematically lower and could indicate the effect of non-Maxwellian profiles and the resulting hot conductivity contribution [18]. This has not yet been studied in detail in TCV as we have concentrated our research on fully non-inductive discharges, that is with zero loop voltage. However, this effect can be important when evaluating the current drive efficiency in discharges with a finite inductive current component. Note also that the evaluation of the different terms is far more accurate in non-inductive discharges as they do not require calculation of the time derivative of the reconstructed equilibrium poloidal flux. From Eqs (4) and (5), it follows that in steady-state fully non-inductive discharges (I_{ohm}=0): $I_{CD} = I_p - I_{BS}$. Typically I_{BS}=20±5kA in the discharges presented here for I_p between 120kA to 210kA. The error bars on I_{BS} are of the order of 25%, therefore the error on the experimental evaluation of I_{CD} is in the range 2.5-5%. The error bars on values calculated by the ray tracing code TORAY [19a] are obviously much larger. TORAY efficiencies, using the COHEN package [19b], are typically 10% to 30% lower than measured [17]. It should not be due to the large velocity approximation [19c] as we obtain similar results with linearized Fokker-Planck calculations with the correct full collision operator. Although this discrepancy remains within the error bars [12], it may indicate a small increase in efficiency due to the formation of an electron tail. This observation is well correlated with measurements by a hard-X ray camera (see Fig. 5) which have revealed a clear high energy tail in CD scenarios. A more detailed study of this effect with Fokker-Planck codes is underway.

The determination of the local driven current is naturally more difficult. However, comparing steady-state fully non-inductive scenarios with all beams in CO-CD with the case with all but one in CO-CD and one in ECH, one obtains the local driven current directly from the difference in the measured total plasma current. This is correct if the power deposition location of the ECH beam is the same as in the CO-CD case, which is obtained within 20% by preparing the launcher angles with TORAY

simulations. In this way, matching the line-averaged density, one can obtain the same density and temperature, (see Fig. 6), and the same bootstrap current profiles. This method was used in Refs [2, 3] to show that there is a strong decrease of the current drive efficiency with increasing minor radius. This effect, which is attributed to particle trapping, is well reproduced by TORAY simulations and has now been confirmed by a recent refined analysis of CD experiments in DIII-D [20]. Note also that the preparation and the analysis of these ECCD discharges have been greatly facilitated by the recent development of a graphical user interface (GUI). This GUI integrates, with a user-friendly interface, the equilibrium and experimental profiles, the launcher geometry and the codes necessary to run TORAY. We have also developed a GUI for the visualisation of the many different parameters related to the TORAY results. This effort has dramatically improved the data interpretation possibilities and the design of experiments.

The steady-state CD pulses in TCV are limited by the gyrotron pulse length. However, as our six gyrotrons are divided into two clusters with independent power generators, we can prolong the discharges by turning on the second cluster at the end of the first cluster pulse. This is shown in Fig. 7, where two gyrotrons of cluster A are used to sustain 100kA of current up to t=2.5s, when they are turned off while two gyrotrons of cluster B are turned on. Note that even though the entire energy and current source is replaced and we are at constant transformer current, there is hardly any perturbation on the plasma parameters, since the beams are aiming at the same ρ locations, albeit at different z positions. This also confirms the stability of these discharges and the accuracy of the beam aiming.

III. Effects of local profile modifications on sawteeth

The main specificity of ECH, besides good coupling and good propagation in both vacuum and plasma, is the short wavelength and the high absorption coefficient resulting in very localised power deposition and current drive density profiles. On the other hand, a characteristic feature of standard tokamak discharges is sawtooth activity, resulting from the internal ideal or resistive kink instability, both of which are very sensitive to the local magnetic shear and to the local pressure gradients near q=1. This has motivated the investigation of the effects of various sawtooth parameters on

the soft-x ray signals, particularly on TCV in view of its flexible EC system [21-24]. We will concentrate here on the effect of local profile modification on the sawtooth period and amplitude. The generic effects are shown in Fig. 8 (solid line) where the sawtooth period increases rapidly at two specific times, corresponding to heating on a well-defined flux surface $\bar{\rho}$ during a vertical sweep of the absorption region. Note that the first peak is smaller and wider than the second one. It has been shown experimentally that the local power density at $\bar{\rho}$, rather than the total power deposited inside $\rho = \bar{\rho}$, is the main parameter correlated with this sawtooth stabilisation [24]. It has also been shown that the small but finite parallel wave number that arises even with injection in the poloidal plane, because of the poloidal magnetic field, is sufficient to drive current; the direction of this current affects the sawtooth period, causing up-down asymmetry. This has been verified by reversing the magnetic field which leads to a sign change in $n_{//}$ and thus a reversal of the order of the peaks shown in Fig. 8 [23]. The sawtooth model [25] included in the $1^1/_2$D transport code PRETOR [26] used for predicting the sawtooth period in the International Thermonuclear Experimental Reactor has been adapted to include electron diamagnetic effects and different regimes of the resistive internal kink growth rate [27]. In this model the condition for triggering a sawtooth crash, $\max(\gamma) > c_* \sqrt{\omega_{e^*}\omega_{i^*}}$, can be re-written as follows [27]: $s_1 > s_{1crit}$, where s_1 is the shear at the q=1 surface and s_{1crit} is a critical shear at q=1 which depends on the local profiles. The value of c_* is currently treated as a free parameter and needs further 3D MHD simulations to characterise it better, in particular to quantify its shape dependence. However, it varies typically between 1 and 1.5 in the ohmic and EC cases studied so far. For the simulations presented here, the value of c_* is chosen to fit the sawtooth period in the ohmic phase and is then kept fixed during the main heating phase [28]. We show in Fig. 8 the PRETOR results of the time evolution of the sawtooth period, as open circles. The qualitative agreement is good in particular on the location of two peaks and on their relative height and width. It should be noted that the simulation is very time consuming as many experimental details have to be taken into account. In particular the effective local power density and current drive values need to be quite accurate. Since the waves are launched in the poloidal plane, the finite value of $n_{||}$ is due to the poloidal magnetic field and therefore depends on the equilibrium reconstruction as well as on an accurate ray-tracing code. We obtain quantitative agreement within the error bars. To better understand the influence of the local current drive, we have simulated two

cases with driven current –3kA and +3kA in a plasma with I_p=330kA (Fig. 9). The sawtooth period changes from 7ms to 11ms, in agreement with TCV results obtained with a local toroidal angle of –4.6° and +7.3° respectively, (solid line in Fig. 9(a)). This allows us to understand the underlying physics mechanisms leading to these modifications. The simulations show that the position $\bar{\rho}$ that maximises the effect on the sawteeth is outside both the q=1 and inversion radii, increases with the power deposition width, and can even be outside the mixing radius [28]. Note that although we use the Kadomtsev model with full reconnection after the crash, a partial reconnection would give the same qualitative effects. When local CO-CD is applied outside q=1, the shear at q=1 takes more time to build up (and less with CNTR-CD) and therefore the sawtooth period is longer (shorter). Local heating has a similar effect because of conductivity increase. Due to the lack of current profile measurements, it is difficult to test this part of the model. However, preliminary analysis indicates that $\bar{\rho}$ is indeed outside the inversion radius and tends to be farther out when the deposition profile is broader [29].

IV. Global profile modifications

As shown in Section II, we are able to non-inductively drive significant currents, sufficient to sustain the whole of the equilibrium current density profile. Therefore global modifications of the current profile are possible, in particular to study the effect of counter-current drive in the centre, in order to obtain flat or reverse shear configuration in quasi steady-state. In Fig. 10 we show a comparison of electron temperature profiles with central heating, CO-CD and CNTR-CD [30]. The lines are results from PRETOR simulations while the data points with error bars are Thomson scattering measurements. There is good agreement between the data and the simulation, which uses the heat conductivity χ_e from the RLW model with constant coefficients [28]. The ECH and the CO-CD cases have similar confinement, which is due to similar sawtooth activity resulting from the peaked current profiles. However, in the CNTR-CD case, the central temperature increases to a much higher level. This is consistent, in both the experiment and the simulation, with the stabilisation of the sawteeth. However, the resulting current and pressure profiles are too peaked and these scenarios terminate with a "monster" sawtooth crash or with an ideal MHD crash.

In order to stabilise this configuration we have added off-axis heating. We have found that by pre-heating the plasmas for about 300ms with only off-axis heating and then adding central CNTR-CD we obtain an improved central electron confinement regime (ICEC) which is stable with or without sawteeth, provided the latter are not too large (see Fig. 11) [10]. The time evolution of the confinement time in such a case is shown in Fig. 12(b) and is compared with a case with central ECH (Fig. 12a). The confinement time is compared with the global RLW scaling [31] which is known to fit the electron energy confinement time in L-modes. Note that in the cases considered here, τ_{RLW} is typically 40% of the L-mode ITER-98 scaling. Using CNTR-CD in the center, values of $H_{RLW}=\tau_{Ee}/\tau_{RLW}$ up to 4 have been obtained. We discuss the heating case first, which already has a very good confinement time ($H_{RLW}=2$). We show in Fig. 13 the time evolution of the central temperature as measured with Thomson scattering (open circles) and as given by the PRETOR simulation. A very good agreement is obtained in all the different phases, namely ohmic, off-axis heating, and off-axis plus central heating. It should be noted that the evolution of the density profile is taken from the measurements in these simulations. This agreement may seem surprising, as PRETOR uses the local RLW χ_e while the experiment exhibits $H_{RLW}\approx 2$ in the latter part of the discharge. To better understand the physics mechanism, we have performed the simulations shown in Fig. 14. We have taken three different power deposition profiles instead of the centrally peaked experimental profile. In addition, we show in Fig. 14(a) (dashed line) the typical χ_e profile. The flat deposition profile, case (a), with only 11% of the total power deposited in the good confinement region, follows the global τ_{RLW} scaling. On the other hand, when a more peaked profile is used, as in case (c) with 87% of P_{tot} inside $\rho=0.3$, a much better global confinement time is obtained, $H_{RLW}=1.8$, even though the same local RLW χ_e is used. The actual power deposition profile for shot 18604 is similar to case (c); for this reason PRETOR can reproduce the temperature profiles correctly even with a high H_{RLW} factor. Note that this effect is encouraging for reactor plasmas as α-heating of the electrons is predicted to be rather peaked, and thus will be concentrated in the good confinement region.

Simulation of the CNTR-CD cases is far more challenging as they exhibit a more dramatic improvement of the internal confinement [10]. This is clearly seen in Fig. 12(b) as there is no further power degradation of τ_{Ee} at the second power step up. In some cases we are nevertheless still able to

reproduce the temperature profile and time evolution (Fig. 15). The profiles in the three phases are well simulated even though the same χ_e expressions are used, that is without any additional reduction.

PRETOR does not successfully reproduce the high confinement regimes in all cases, as evidenced by the case shown in Fig. 16. In order to clarify whether this discrepancy is due to the transport model or to changes in the experimental profiles, we have changed the location of the central deposition from $\rho=0$ to $\rho=0.2$, that is within the error bars of the TORAY results and the equilibrium reconstruction. We show in Fig. 17(a) the resulting variation in the central q profile, using the experimental n_e and T_e profiles, loop voltage and assuming steady-state profiles according to Eq. (2). One sees that q can vary from flat or monotonic to deeply reversed. The current profiles resulting in the dashed q profile are shown in Fig. 17(b). This illustrates the difficulty in simulating these discharges. Indeed the high central temperature leads to very good CNTR-CD efficiency, that is to a large negative j_{CD} contribution, such that $|I_{CD}|>0.5I_p$. To compensate this current, a large centrally peaked ohmic current is generated. Therefore the total current profile is the result of the difference of two large contributions. Moreover a slight shift of the peaked j_{CD} to an off-axis position, i.e. to $\rho\approx0.1$, or a change in the deposition width changes the total current profile considerably. The fact that PRETOR can simulate the improved central confinement is mainly due to the possibility to obtain a reverse shear and a low q profile: since χ_e increases with $q/|s|$, where $|s|$ is the absolute value of the magnetic shear, a large shear (negative or positive) is beneficial. Note that the favourable negative shear dependence is also predicted by recent gyro-kinetic simulations [32]. As we have a wide range of q profiles consistent, within the error bars, with the experimental measurements, we cannot validate or invalidate the model. However, a testable prediction of the model is the high sensitivity of τ_{Ee} to changes in the power deposition location of the central gyrotrons. Preliminary experiments have been performed to test this effect. We show in Fig. 18 the comparison between two discharges whose only difference is a 3^o variation in the poloidal launcher angles of the central beams. We see that shot 19428 does not reach the improved internal confinement regime and actually the central temperature values are consistent with the unsuccessful PRETOR simulation of shot 18639, shown earlier in Fig. 16.

V. Conclusions

We have clearly demonstrated the steady recharging of the transformer with ECCD alone, for more than 10 current redistribution times τ_{crt}. We have also improved our full current replacement discharges by using a feedback control on the transformer current which ensures that no inductive current is driven. With this technique and distributing six gyrotron beams across the plasma minor radius, we have driven up to 210kA in a steady-state, fully non-inductive discharge with P=2.7MW, $n_{el} \approx 1.3 \cdot 10^{19} m^{-3}$, $T_{e0} \approx 5keV$, $I_{BS} \approx 20kA$. These discharges are designed to be stable by pre-programming a sufficiently broad power deposition profile. This external control was further demonstrated by switching between two sets of gyrotron beams, aiming at similar ρ locations.

We have presented the effect of small localised current drive, totalling less than 1% of the plasma current, on the sawtooth period. These local profile modifications are accurately simulated by a sawtooth model included in PRETOR which triggers a crash if the shear at q=1 is larger than a critical shear dependent on the local profiles.

We have studied the effect of global profile modifications on energy confinement. We have shown that global confinement scalings have limited applicability even when the underlying heat conductivity model is robust when highly localised power sources are present. In particular we obtain good global confinement with peaked central heating as most of the power is deposited in the good confinement region. Adding counter-current drive in the centre further improves the internal confinement. This is consistent with the generation of reverse shear within the constraints of the RLW χ_e model. The fact that an off-axis pre-heating phase of about one to two τ_{crt} is needed in order to obtain this improved central electron confinement regime (ICEC) is further evidence of the important role of the q profile. Finally the high sensitivity of τ_{Ee} to the deposition location, through its effect on the q profile, which was predicted by PRETOR simulations, has been confirmed experimentally.

Acknowledgments

This work was supported in part by the Swiss National Science Foundation.

References

1 F. Hofmann, J.B. Lister, M. Anton et al., Plasma Phys. Control. Fusion **36**, B277 (1994).

2 O. Sauter, R. Behn, S. Coda *et al*, Proc. 26th EPS Conference on Control. Fusion and Plasma Physics, Maastricht, 1999, edited by B. Schweer (Europhys. Conf. Abstr., 1999), Vol. 23J, p. 1105.

3 O. Sauter, M.A. Henderson, F. Hofmann *et al*, Phys. Rev. Lett. **84**, 3322 (2000); "*Steady-state fully noninductive current driven by electron cyclotron waves in a magnetically confined plasma*" to be published in Fusion Eng. Design.

4 A. Ando, K. Ogura, H. Tanaka et al., Phys. Rev. Lett. **56**, 2180 (1986)

5 H. Tanaka, K. Ogura, A. Ando *et al*, Nucl. Fusion **31**, 1673 (1991)

6 V.V. Alikaev, A.A. Bagdasarov, A.A. Borshegovskij *et al*, Nucl. Fusion **32**, 1811 (1992).

7 B. Lloyd, Plasma Phys. Control. Fusion **40**, A119 (1998).

8 D. A. Kislov, V.V. Alikaev, Yu.V. Esipchuk, A.M. Kakurin, A.Ya. Kislov, D.A. Martynov, G.E. Notkin, K.A. Razumova, A.V. Sushkov, V.V. Volkov, Nucl. Fusion **37**, 339 (1997).

9 G. Gantenbein, H. Zohm, G. Giruzzi, S. Günter, F. Leuterer, M. Maraschek, J. Meskat, Q. Yu, ASDEX Upgrade Team, and ECRH-Group (AUG), Phys. Rev. Lett. **85**, 1242 (2000).

10 Z.A. Pietrzyk, C. Angioni, R. Behn, S. Coda, T.P. Goodman, M.A. Henderson, F. Hofmann, O. Sauter, "*Long-pulse improved central electron confinement in the TCV tokamak with electron cyclotron heating and current drive*", to be published in Phys. Rev. Lett.

11 N. J. Lopes Cardozo, G. M. D. Hogeweij, M. de Baar *et al*, Plasma Phys. Control. Fusion **39**, B303 (1997).

12 S. Coda, T.P. Goodman, M.A. Henderson *et al*, Plasma Phys. Control. Fusion **42** B311 (2000).

13 H. Weisen for the TCV Team, "*Overview of TCV results*", to be published in Proceedings of the 18th International Conference on Plasma Physics and Controlled Nuclear Fusion Research, Sorrento, 2000 (International Atomic Energy Agency (IAEA), Vienna, 2001).

14 S. Coda, Y. Peysson, L. Delpech *et al*, ibid. [2], p. 1097.

15 F.L. Hinton and R. D. Hazeltine, Rev. Mod. Phys. **48**, 239 (1976).

16 O. Sauter, C. Angioni and Y.R. Lin-Liu, Phys. Plasmas **6**, 2834 (1999).

17 P. Nikkola and O. Sauter, "*Numerical and experimental studies of ECCD efficiency in plasmas with nearly zero ohmic current*", in Proc. of the Theory of Fusion Plasmas workshop, Varenna 2000 (Editrice Compositori E. Sindoni, Bologna, 2000).

18 N.J. Fisch, Phys. Fluids. **28**, 245 (1985).

19 G. Smith, L. D. Pearlstein, A. H. Kritz, I. P. Shkarofsky, A. Pochelon, A. Hirt, O. Sauter, T. Goodman, G. Giruzzi and J. L. Segui, in *Proceedings of the 9th Joint Workshop on ECE and ECRH*, Borrego Springs, CA, 1995, edited by J. Lohr (World Scientific, Singapore, 1995), p. 651; R. H. Cohen, Phys. Fluids **30**, 2442 (1987); E. Westerhof, ibid. [19a], p. 3

20 Y. R. Lin-Liu, Bull. Amer. Phys. Soc. 45, 213 (2000).

21 Z.A. Pietrzyk, A. Pochelon, T.P. Goodman *et al*, Nucl. Fusion **39**, 587 (1999).

22 I. Furno, C. Angioni, F. Porcelli, H. Weisen, R. Behn, T.P. Goodman, M.A. Henderson, Z.A. Pietrzyk, A. Pochelon, H. Reimerdes, "*Understanding sawtooth activity during intense electron cyclotron heating experiments on TCV*", to be published in Nucl. Fusion.

23 M. Henderson, T.P. Goodman, F. Hofmann, S. Coda, I. Furno, J.–P. Hogge, Z.A. Pietrzyk, H. Reimerdes, J. Rommers, "*Poloidally asymmetric plasma response with ECH deposition near q=1 in TCV*", to be published in Fusion Engineering and Design.

24 T. Goodman, M.A. Henderson, J.-P. Hogge, Z.A. Pietrzyk, A. Pochelon, O. Sauter, in idib. [2], p. 1101.

25 F. Porcelli, D. Boucher and M. N. Rosenbluth, Plasma Phys. Control. Fusion **38**, 2163 (1996).

26 D. Boucher and P. H. Rebut, in Proc. International Atomic Energy Agency (IAEA) Tech. Conf. on Advances in Simulation and Models of Thermonuclear Plasmas, Montreal (IAEA, Vienna, 1992) p. 142.

27 O. Sauter, C. Angioni, D. Boucher, I. Furno, A. Pochelon, F. Porcelli, in Proceedings of the Theory of Fusion Plasmas workshop, Varenna 1998 (Editrice Compositori E. Sindoni, Bologna, 1998) p. 403.

28 C. Angioni, T.P. Goodman, Z.A. Pietrzyk, O. Sauter, "*Simulations of improved confinement discharges and sawtooth period with electron cyclotron heating and currrent drive in TCV*", ibid. [17].

29 T. Goodman, M. Henderson, C. Ancioni, S. Coda, I. Furno, P. Nikkola, H. Reimerdes, O. Sauter, Bull. Amer. Phys. Soc., Vol. 45, p. 53 (2000).

30 Z. A. Pietrzyk, C. Angioni, Behn, *et al*, Phys. *Plasmas* **7**, 2909 (2000).

31 P. H. Rebut *et al*, in Proceedings of the 12th International Conference on Plasma Physics and Controlled Nuclear Fusion Research, Nice, 1988 (International Atomic Energy Agency (IAEA), Vienna, 1989), Vol. 2, p. 191.

32 F. Jenko, Phys. Plasmas **7**, 1904 (2000).

Figure captions.

Figure 1. Examples of plasma shapes used in the 2000 campaign. Some TCV parameters: $I_p<1$MA (design 1.2MA), $R_0=0.88$, $a=0.25$m, $B_0<1.54$T, $0.9\leq\kappa\leq2.8$, $-0.5<\delta<0.9$. TCV has two in-vessel fast control coils.

Figure 2. Range of angles in both poloidal and toroidal planes for the top and equatorial beams. One of the angles can be changed during a shot.

Figure 3. Steady recharging of the transformer with two gyrotrons, P=0.9MW, for 1.6s [3a].

Figure 4. Steady-state fully non-inductive current record discharge with $I_{CD}=190$kA and $I_{BS}=20$kA. The feedback to keep the transformer current I_{OT} constant is turned on at t=1.1s. The pulse is limited only by the gyrotron pulse length.

Figure 5. Hard X-ray emissivity in heating and CO-CD cases. The ECH case does not show any non-Maxwellian feature, while the CO clearly does.

Figure 6. Temperature and density profiles for two discharges each with 3 gyrotrons distributed over the minor radius. The only difference is that the gyrotron aiming at z=12cm is in CO-CD position for shot 19708 and in ECH position for 19710. The line-averaged density was higher in the first case by less than 5%.

Figure 7. Steady-state fully non-inductive discharge where the first set of gyrotrons are all switched off at 2.5s and a second set is switched on, aiming at the same ρ. Even though the whole energy and current sources are turned off and on, while keeping I_{OT} constant, the plasma stays in steady-state.

Figure 8. The resonance location is swept during the shot in the vertical direction, with one gyrotron, crossing twice the q=1 flux surface. The solid line shows the experimental sawtooth period, while the dots are the PRETOR results. The location of the peaks are in good agreement with the experiment, well within the error bars on TORAY local power deposition profile and current drive

Figure 9. Simulation of the effect of a gyrotron beam with about 5^o toroidal angle. The magnitude of the increase of the sawtooth period is in good agreement with experimental results marked with a short solid line.

Figure 10. Temperature profiles as obtained from the Thomson scattering system (data with error bars) compared with the results of PRETOR. The top curve corresponds to the CNTR-CD case which suppressed the sawtooth activity for about 100 ms [30].

Figure 11. Temperature profiles with their fits for cases where the target plasma is pre-heated with an off-axis beam. Adding central CNTR-CD dramatically improves the central confinement: P_{tot}=2.25MW, shot 18518 (solid line), and P_{tot}=1.8MW, shot 18639 (dashed line). Adding only central heating , P_{tot}=2.25MW (18604), yields much lower central temperature.

Figure 12. Time evolution of the electron energy confinement time as compared with the RLW global scaling law. Shot 18604 corresponds to the bottom curve in Fig. 11, while shot 18518 corresponds to the top one.

Figure 13. Central temperature (T_{e0}) time evolution from Thomson data and as obtained with PRETOR for the case with only ECH heating (Fig. 12(a)). PRETOR follows accurately the whole time evolution while the factor H_{RLW} increases from 1 in ohmic to 2 in the latter phase.

Figure 14. Simulation of the effect of changing only the power deposition profile, towards peaked central heating. H_{RLW} steadily increases when most of the power is in the low χ_e region.

Figure 15. (a) Time evolution of T_{e0} as obtained from Thomson scattering data and from PRETOR. Shot 18518 corresponds to the top curve of Fig. 11. (b) The corresponding profiles are shown, where the lines are the PRETOR results.

Figure 16. Time evolution of T_{e0} for the shot 18639. PRETOR does not obtain an improved internal confinement regime after the central beams are turned on.

Figure 17. (a) Range of possible q profiles as obtained in PRETOR using the experimental density and temperature profiles and varying slightly the power deposition location with respect to the TORAY results. (b) Contributions to the current profile corresponding to the dashed q profile in (a), which is obtained with on-axis CNTR-CD as indicated by the j_{CD} profile.

Figure 18. Time evolution of T_{e0} for a case similar to 18639, shot 19421, and then changing the poloidal angle of the two central beams by only 3°. The second case does not establish the ICEC regime

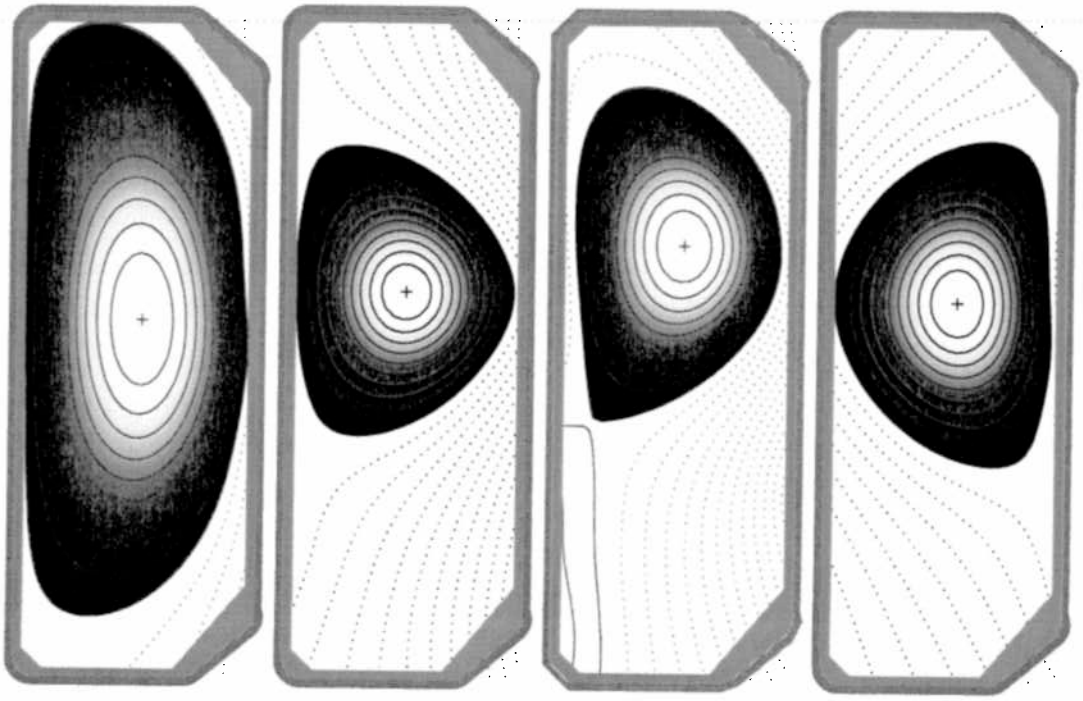

Figure 1

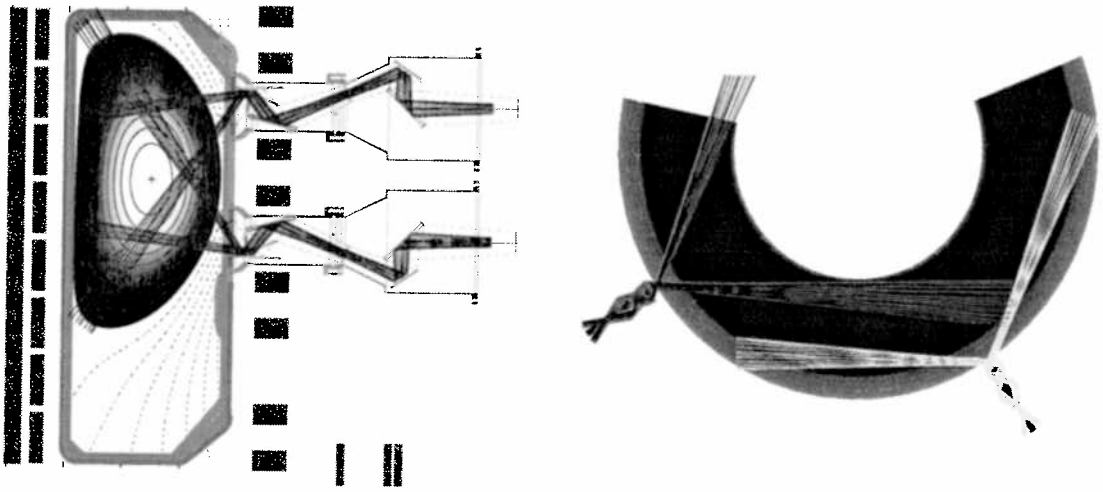

Figure 2

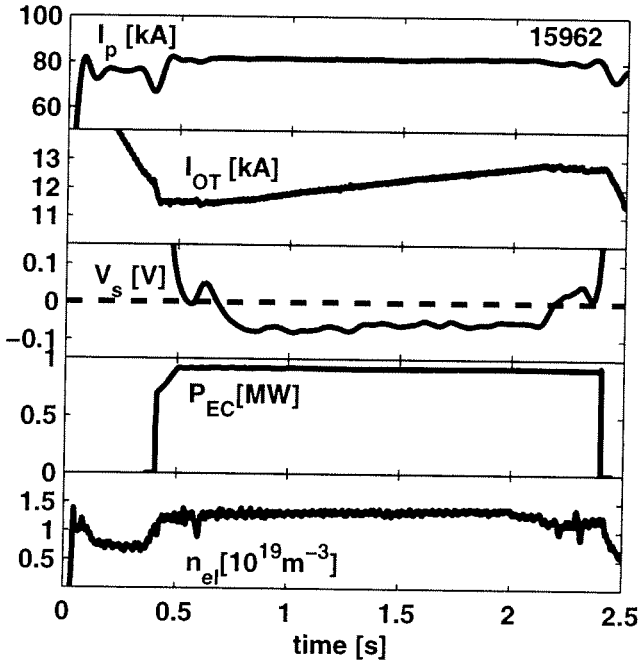

Figure 3

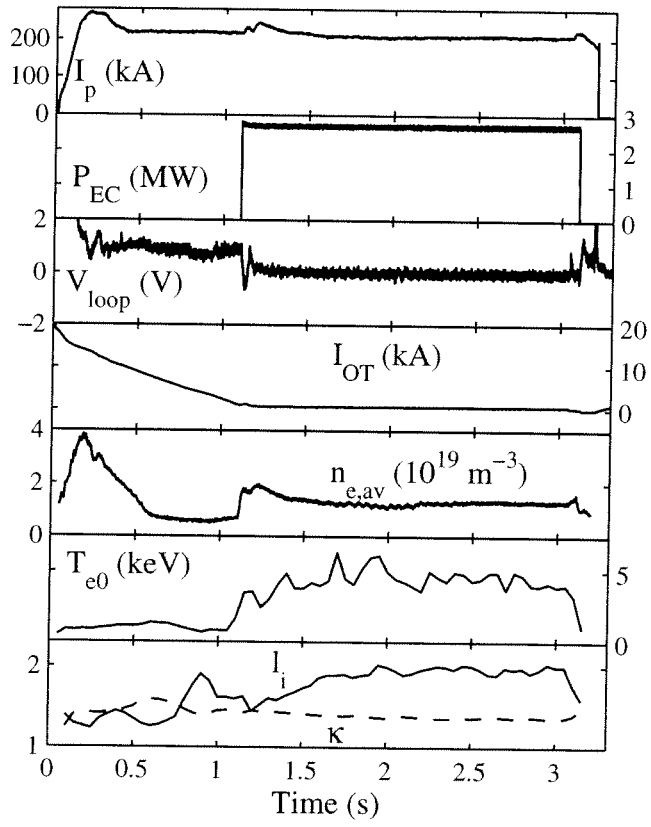

Figure 4

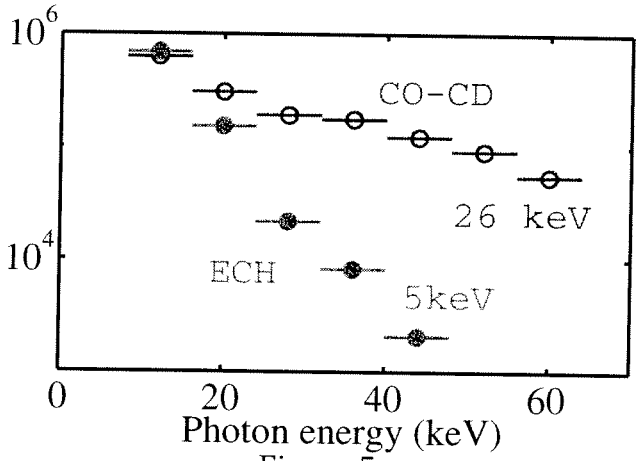

Figure 5

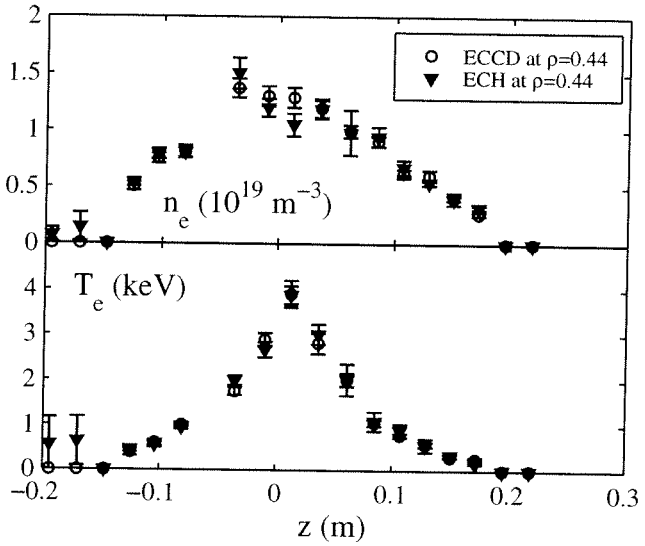

Figure 6

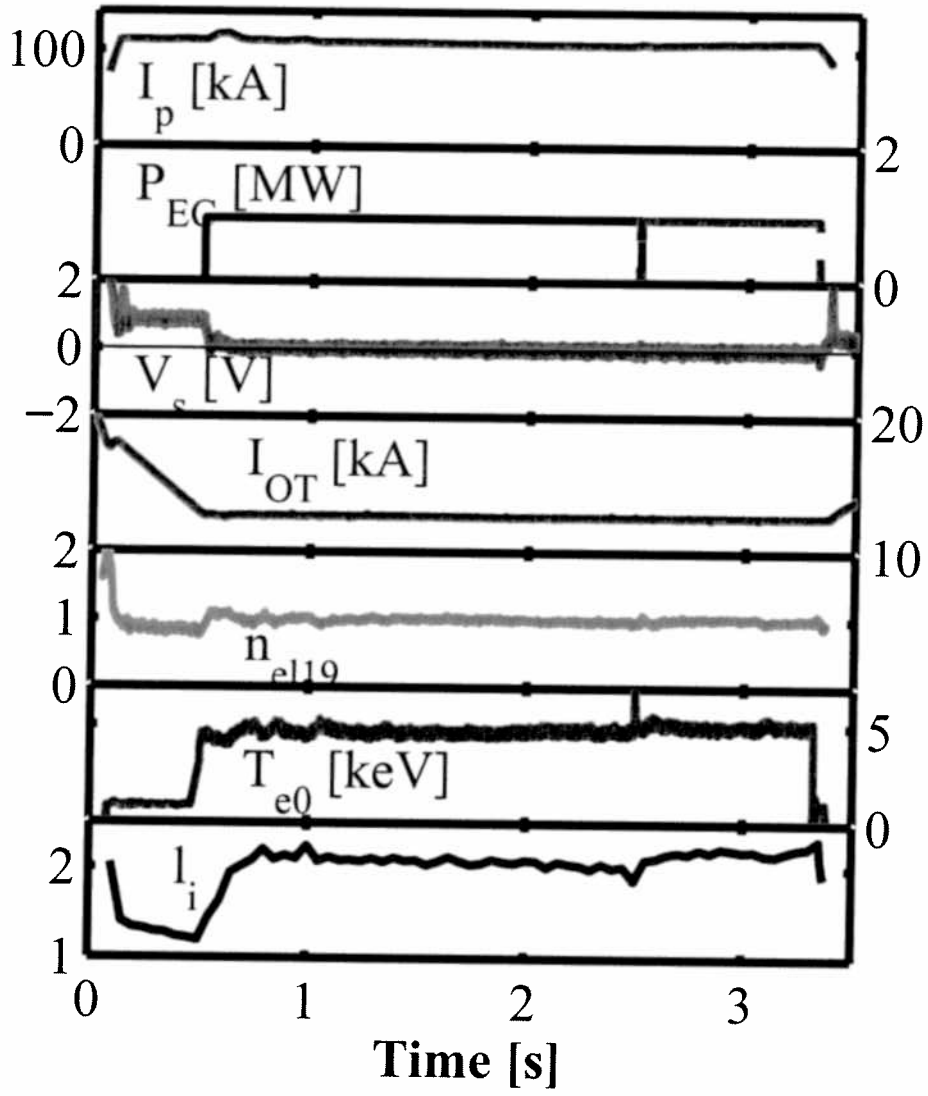
100
0
I_p [kA]
P_{EC} [MW]
2
0
2
0
V_s [V]
−2
I_{OT} [kA]
20
2
1
0
10
n_{el19}
T_{e0} [keV]
5
0
2
1
l_i
0
1
2
3
Time [s]

Figure 7

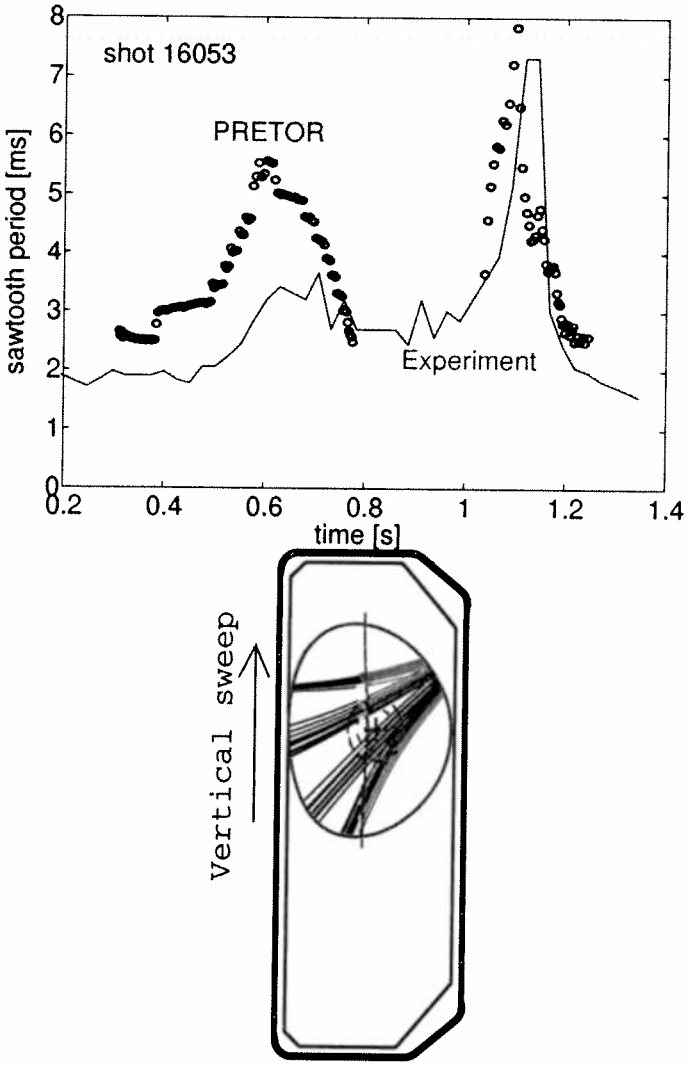

Figure 8

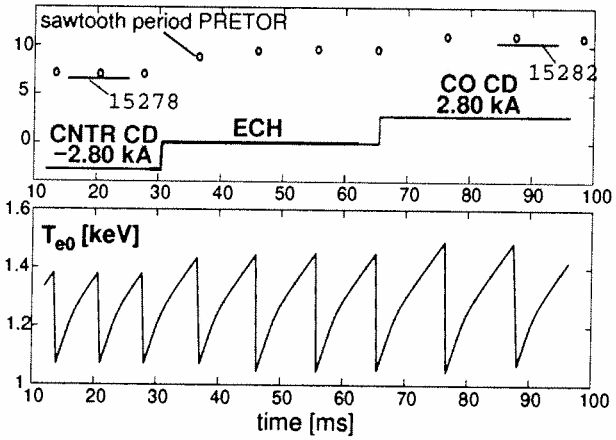

Figure 9

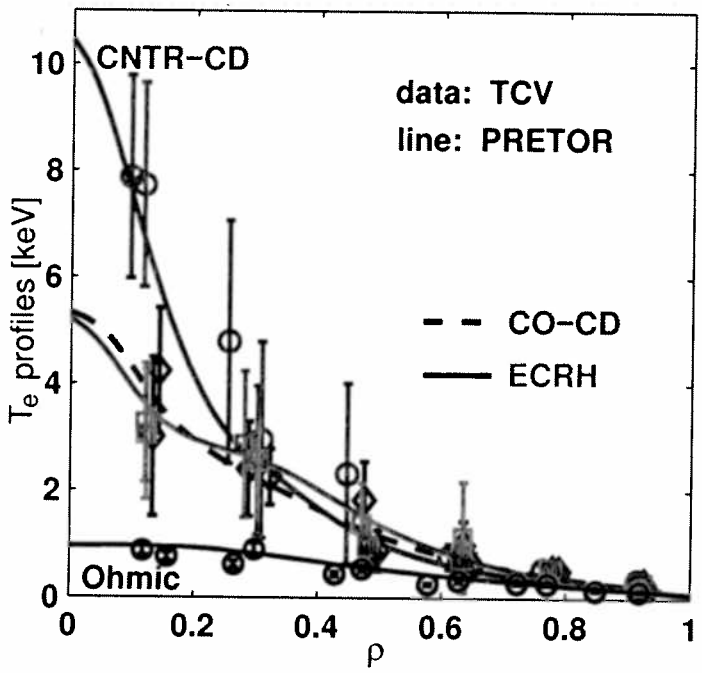

Figure 10

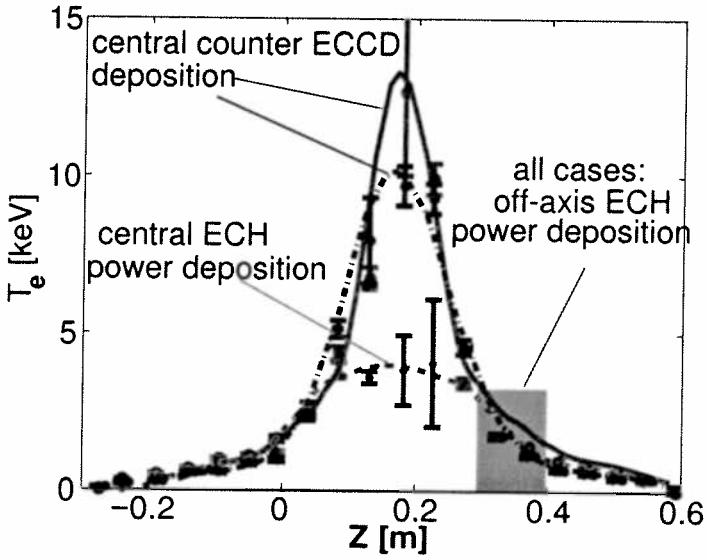

Figure 11

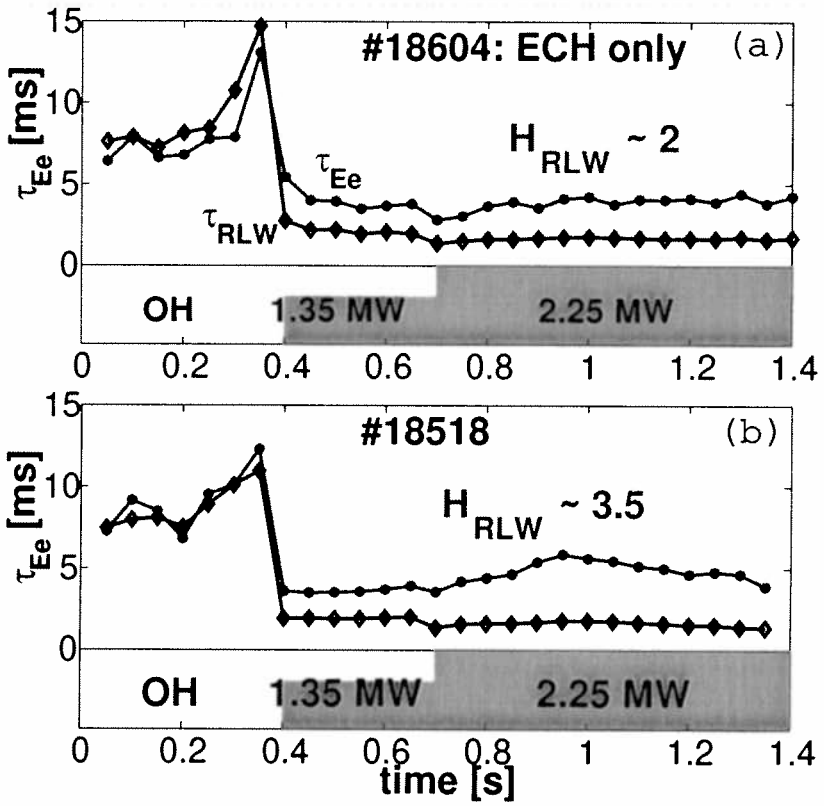

Figure 12 (a), (b)

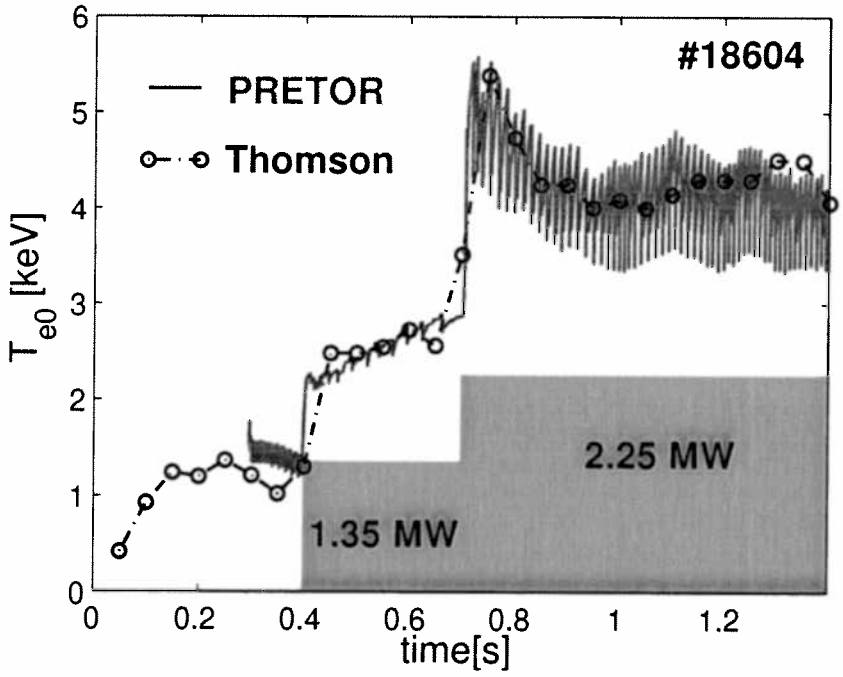

Figure 13

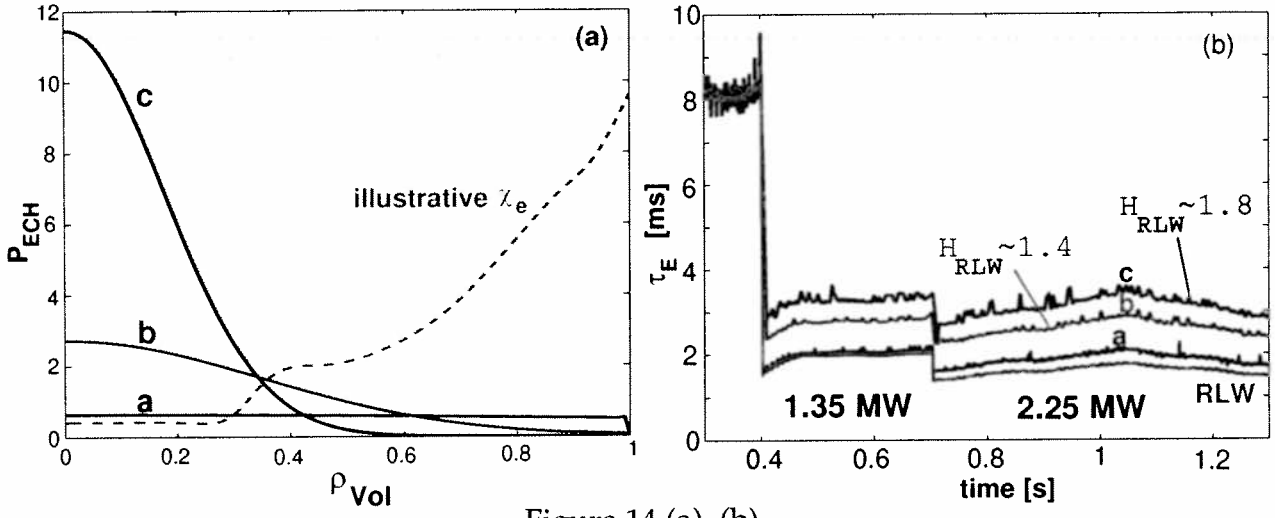

Figure 14 (a), (b)

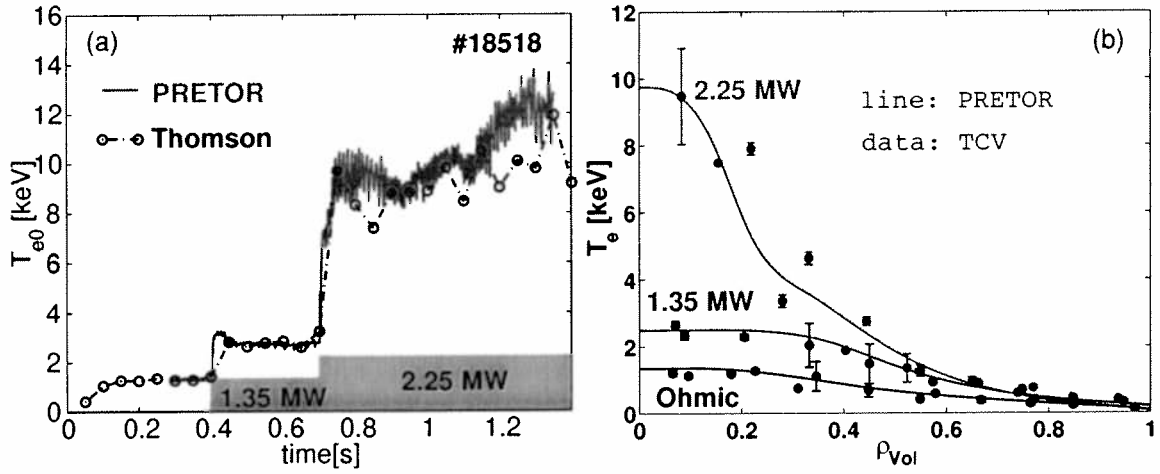

Figure 15 (a), (b)

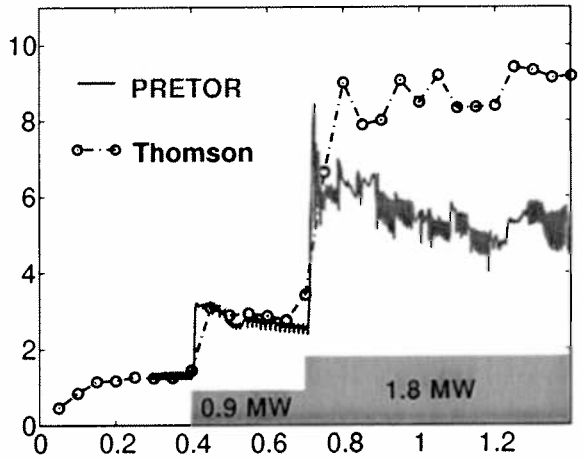

Figure 16

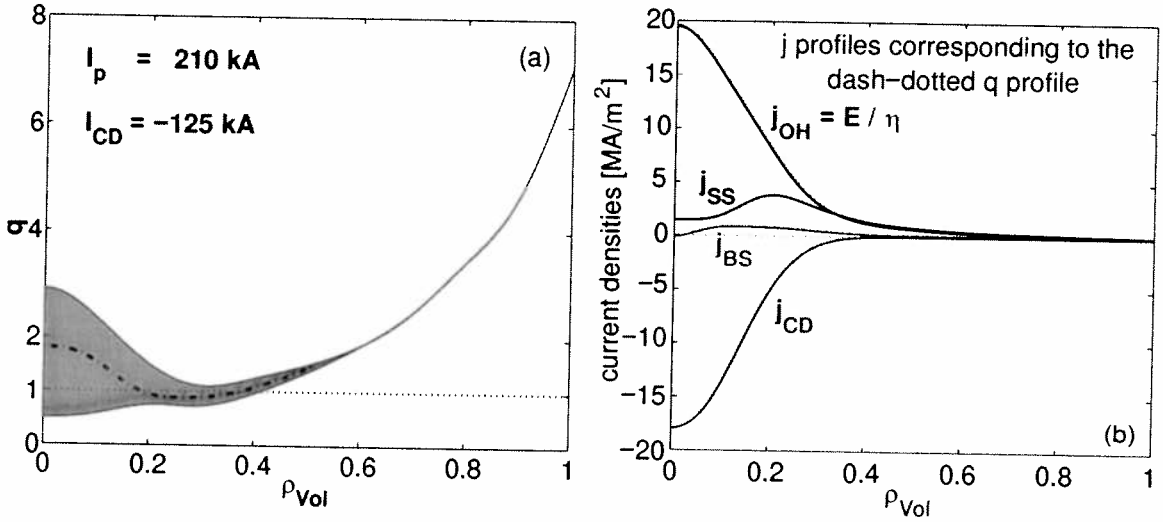

Figure 17 (a) , (b)

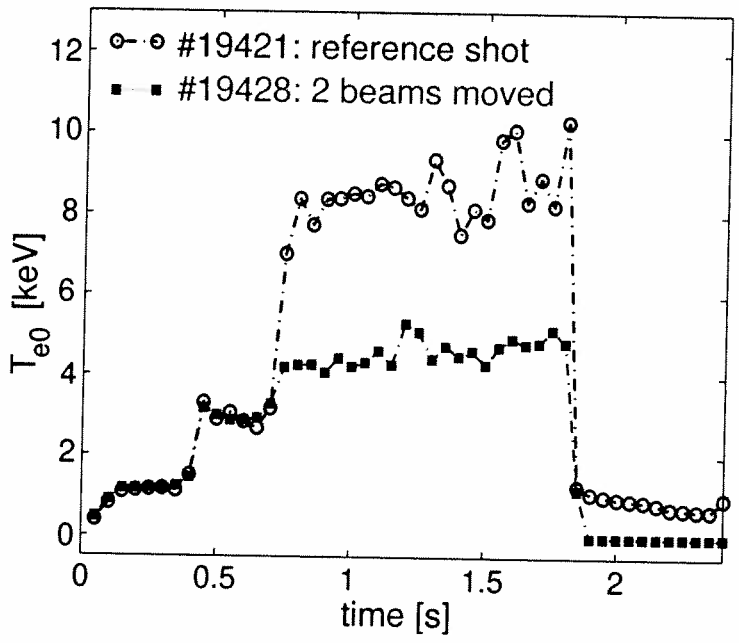

Figure 18